CHAPTER 4

THERMODYNAMIC PREDICTION OF THE LIQUIDUS, SOLIDUS, AND AE3 TEMPERATURES, AND PHASE COMPOSITIONS FOR LOW-ALLOY MULTICOMPONENT STEELS

4.1 INTRODUCTION

The vast majority of steel weld deposits solidify under highly nonequilibrium cooling conditions. A consequence of this is the chemical segregation of substitutional alloying elements during solidification, a segregation that persists as the weld cools to ambient temperature. Solidification-induced segregation of interstitials is usually not a problem due to the ease with which they can diffuse and homogenize during cooling. The presence of substitutional element segregation can greatly influence the subsequent transformation of austenite into ferrite with reaction kinetics in general being accelerated in the solute-depleted regions. The formation of ferrite in these regions causes a redistribution of carbon into the remaining austenite whose hardenability is therefore increased. It has been demonstrated that such effects can have a major influence on the development of microstructure (Gretoft *et al.*, 1986), and any method for alloy design must take them into proper consideration.

Weld metal compositions typically solidify as delta-ferrite (δ), and subsequently transform to austenite (γ), and then to ferrite (α). In order to obtain a general model for the prediction of the properties of a weld metal, it will be necessary to be able to predict the chemical segregation behaviour during solidification. For low-alloy C-Mn steel weld deposits solidifying as δ-ferrite, the solute-enriched prior δ-boundaries will finish up approximately within the centre of the austenite grains. The effect of the segregation will be to raise the temperature at which allotriomorphic ferrite first forms, and to increase the temperature range over which, α forms. Hence, the ultimate volume fraction for a given set of cooling conditions will increase (Strangwood and Bhadeshia, 1987). Conversely, for solidification as austenite, since regions in the proximity of the austenite boundaries would be solute-enriched, nucleation of α would be expected to be more difficult (Gretoft *et al.*, 1986). To predict weld metal segregation quantitatively will necessarily require a knowledge of the solidification temperature, solidification range, degree of parti-

tioning in the melt, and partition coefficients for the carbon and solute elements in the steel. This work is an attempt at modelling the high temperature region of the phase diagram for multicomponent steels using the general thermodynamic techniques developed by Kirkaldy and co-workers (Baganis and Kirkaldy, 1978; Kirkaldy, 1978). In order to check the consistency of the calculations, and of the thermodynamic data used, calculations were also attempted for the α/γ equilibria, where the amount of experimental data available as a check of theory is far greater.

4.2 THE SOLIDIFICATION OF STEEL

The solidification of steel can take place in three ways:

- primary ferrite formation;
- primary ferrite formation followed by a peritectic reaction;
- primary austenite formation

For most low-alloy steel weldments, solidification entails a peritectic transformation (Figure 4.1). In plain carbon steels, the high diffusivity of carbon at the peritectic temperature means that the peritectic reaction is very rapid, and all of the primary dendrites transform to the more stable austenite. However, quenching specimens from $\gamma/\delta + L$ field has shown there to be considerable residual melt between solidified dendrites, and, in some steels, evidence of this may be seen in the completely solidified structure (Erokin *et al.*, 1960). At higher carbon contents, the primary crystals are δ, but just below 1500°C, a peritectic reaction takes place, and the remainder of the weld solidifies as austenite.

The mechanism of solidification, and in particular the peritectic reaction, in iron-base alloys has been investigated most recently by Fredriksson and his co-workers using unidirectionally solidified steels (Fredriksson, 1976; Fredriksson and Stjerndahl, 1982). Metallographic and microprobe analysis of quenched samples allowed the solidification process to be analysed. It was found that ferrite-stabilizing elements can segregate strongly to the ferrite during solidification. Austenite-stabilizing elements favour a peritectic reaction during the solidification process and ferrite-stabilizing elements favour a eutectic reaction (Fredriksson, 1977). Experimental and theoretical work (Sterenbogen *et al.*, 1976; 1977) indicates that the greatest influence on the mode of solidification and the dimensions of the two phase region in the welding of steel is that exerted by carbon whose concentration must

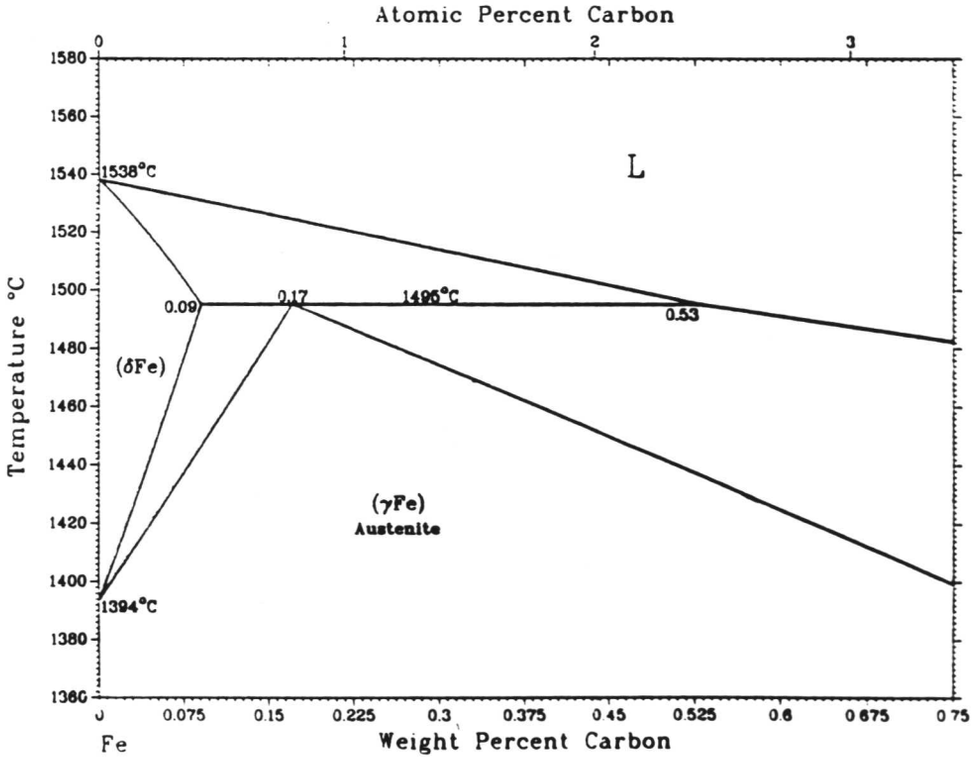

Figure 4.1: Peritectic region of the Fe-C phase diagram. (After "Binary Alloy Phase Diagrams", Ed., T. B. Massalski, American Society for Metals, Ohio 44073, Vol. 1, 563).

therefore be known the most accurately. The carbon content largely controls the constitutional supercooling of the system. The peritectic reaction is influenced by the diffusion rate of the different alloying elements in austenite as well as in ferrite. This in turn will influence segregation behaviour. For a fixed carbon content, adding an alloying element will either expand or contract the γ-field, too. Most iron-base alloys contain one or more austenite-stabilizing elements (*e.g.* C, Ni, Mn) and one or more ferrite-stabilizing elements (*e.g.* P, Cr, Mo).

The segregation behaviour of an alloying element can be characterised using the segregation ratio S, defined as the local maximum in alloy content divided by the local minimum. The calculation of the segregation ratio for primary precipitation of ferrite as been made by Fredriksson and Stjerndahl (1982), the major assumptions being negligible undercooling from radius of curvature effects, no macrosegregation, complete diffusion in the liquid in interdendritic spaces, and equilibrium in the liquid at the solid-liquid interface. It is assumed (Fredriksson, 1976; Fredrikkson, 1977) that the lever rule describes the solidification process during primary precipitation of ferrite. Let $C_s(t)$ be the solute concentration at the solid-liquid interface. Then, by using a mathematical model derived from homogenization of a cast structure (Kattamis and Flemings, 1965; Purdy and Kirkaldy, 1971), the concentration distribution as a function of time can be described by the relation

$$C(x,t) = C_s(t) - (C_s(t) - C_o\mathrm{k}) \exp -\frac{\pi^2}{\lambda^2} Dt \sin \frac{\pi x}{\lambda} \tag{4.1}$$

t is the holding time

and x is the distance from $x = 0$ to $x = \lambda$.

The symbols used are defined in Figure 4.2. At the end of the solidification process the concentration distribution is sinusoidal, the wavelength being twice the distance between the primary plates. In this case, since the diffusion rate in ferrite is rather high, the largest possible wavelength is chosen. Then, C_s is given by the following material balance

$$C_o.\lambda = C_o \int_0^{\lambda} (C_S(t) + (C_s(t) - C_o k)) \exp -\frac{D\pi^2 t}{\lambda^2} \sin \frac{\pi x}{\lambda}\, dx \tag{4.2}$$

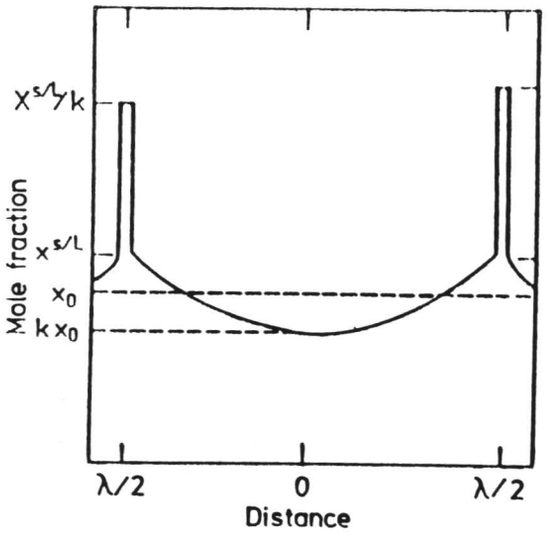

Figure 4.2: Theoretical distribution of alloying elements for calculations of segregation ratio. (After H. Fredriksson and J. Stjerndahl (1982), *Met. Sci.*, **16**, (12), 577).

which gives

$$C_s(t) = C_o \cdot \frac{1 - \left[(2\mathrm{k}\exp - \frac{D\pi^2 t}{\lambda^2})/\pi\right]}{\left(1 - \frac{2}{\pi}\exp - \frac{D\pi^2 t}{\lambda^2}\right)} \tag{4.3}$$

Using Eqns. 4.1 and 4.3, the segregation ratio becomes

$$S = \frac{1}{\left\{1 - \left[\frac{1 - \mathrm{k}(1 - \frac{2}{\pi}\exp - \frac{D\pi^2 t}{\lambda^2})}{1 - \frac{2\mathrm{k}}{\pi}\exp - \frac{D\pi^2 t}{\lambda^2}}\right]\right\}\exp - \frac{D\pi t}{\lambda^2}} \tag{4.4}$$

To calculate the segregation ratio one must know the solidification time and the dendrite plate space. However, if one assumes a constant cooling rate, they can be related thus:

$$t = \Delta\mathrm{T}/\left(\frac{dT}{dt}\right) \tag{4.5}$$

$$\text{and} \quad \lambda = A\left(\frac{dT}{dt}\right)^n \tag{4.6}$$

where ΔT is the solidification range, and A and n are experimentally determined constants. Substituting in Eqn. 4.4 then gives

$$S = \frac{1}{1 - \left\{ \frac{1 - \mathrm{k}(1 - \frac{2}{\pi} \exp - \frac{\pi^2 D\Delta T}{A^2 \left(\frac{dT}{dt}\right)^{1+2n}})}{1 - \frac{2\mathrm{k}}{\pi} \exp - \frac{\pi^2 D\Delta T}{A^2 \left(\frac{dT}{dt}\right)^{1+2n}}} \right\} \exp - \frac{\pi^2 D\Delta T}{A^2 \left(\frac{dT}{dt}\right)^{1+2n}}} \tag{4.7}$$

For primary precipitation as austenite, segregation behaviour can be calculated approximately starting from the modified Scheil equation first derived by Flemings *et al.* (1966) to give

$$S = \left(\frac{1 + \{\mathrm{k}\, D\Delta T / [(dT/Dt)^{1+2n} A^2]\}}{\mathrm{k}\, D\Delta T / [(dT/dt)^{(1+2n)} A^2]} \right)^{(1-k)} \tag{4.8}$$

Thus, it can be seen that, in both cases, for a constant cooling rate, the amount of segregation experienced in steels for solidification as either ferrite or austenite can be directly related to the solidification range of the alloy and the partition ratios of the solute elements.

4.3 METHOD OF ANALYSIS

One of the most important factors which needs to be considered in the thermodynamic modelling of the Fe-C-X multicomponent system is that it ceases to retain the characteristics of infinite dilution for concentrations above about 0.2 wt%C (Darken and Gurry, 1953; Schürmann *et al.*, 1987). In the analysis of Baganis and Kirkaldy (1978), which is used in the present work, this problem is circumvented by determining the temperature deviation of a particular phase boundary from the corresponding boundary in the binary Fe-C system. The change in carbon concentration at a phase boundary, due to the addition of substitutional alloying elements, is given by summing the effects due to each individual element. The large amount of thermodynamic data on Fe-X and Fe-C-X systems that has been accumulated over the last 20 years makes it possible to carry out these thermodynamic calculations with high accuracy.

In the following description, Fe is designated as zero, C as 1, and the alloying elements Si, Mn, Ni, Cr, Mo, Cu, V, Nb, Co, W as i(=2 to n) respectively. The mole fractions in each phase are designated as X_i(i=0 to n). A general temperature coordinate system on a phase boundary in the pure Fe-C system is designated $T_\circ$. The temperature deviation from $T_\circ$ due to the addition of substitutional alloying elements, ΔT, is calculated for the required range of $T_\circ$, so that the phase boundary, T{Fe-C-X(i)}, may be found. This procedure follows the classical "depression of the freezing point" relation due to Van't Hoff [see Darken and Gurry (1953), 222-224]. In multicomponent alloys, the temperature changes due to individual allou additions, are additive, so long as solute-solute interactions are taken as negligible. The interactions between elements in solution are represented by ϵ_{ik} are empirical coefficients known as the Wagner interaction parameters, and the above assumption of additive ΔT values is the same as saying that the interaction between elements i and k, $\epsilon_{ik}(i \neq k,\ i \text{ and } k > 1) = 0$. In fact, this is not strictly correct (Kagawa *et al.*, 1985), and silicon, especially, can interact with other solute elements (Craska and McLellan, 1971). However, Kirkaldy and his co-workers found that this assumption is valid so long as the total alloying element content is less than about 6wt% and the silicon content is less than 1wt%.

In order to calculate the temperature deviation at a phase boundary, ΔT, Baganis and Kirkaldy (1978) started with the relationship for the equality of the chemical potentials in the two phases which are in equilibrium. For example, for the austenite + liquid/liquid phase boundary, for Fe

$$X_\circ^\gamma \gamma_\circ^\gamma = X_\circ^L \gamma_\circ^L \exp\left(\frac{\Delta^\circ G_o^{\gamma \to L}}{RT}\right) \tag{4.9}$$

where $X_\circ = 1 - \sum X_{i=1}^n$, is the mole fraction of iron, and $\gamma_\circ$ is the activity coefficient for the iron for which the superscripts γ and L denote the austenite and liquid phases respectively.

$\Delta^\circ G^{\gamma \to L} = {}^\circ G_L - {}^\circ G_\gamma$, or, more generally, the difference between the Gibbs free energies of the pure higher and lower temperature phases.

and T is the phase boundary temperature.

Similarly for C($n = 1$) or component i

$$X_i^{\gamma}\gamma_i^{\gamma} = X_i^{L}\gamma_i^{L}\exp\left(\frac{\Delta^{\circ}G_i^{\gamma\rightarrow L}}{RT}\right) \tag{4.10}$$

The Wagner-Taylor expansions for the activity coefficients (Wagner, 1952) were then substituted into Eqns. 4.10 and 4.11. Eventually, this gave the temperature deviation in the form

$$\Delta T = RT_{\circ}^{2}\sum_{i=2}^{n} A_i X_i^{L} \tag{4.11}$$

where X_i^L is the mole fraction of component i,

and where

$$A_i = \frac{\left[A_i^{\circ} - \{(1 + X_1^L(1 - X_1^L).(\epsilon_{1i}^L - \epsilon_{11}^{\gamma}A_1^{\circ}A_i^{\circ})\}\exp\{\frac{\Delta^{\circ}G_{\circ}}{RT_{\circ}^2} - (\frac{X_1^L}{2})(\epsilon_{11}^L - \epsilon_{11}^{\gamma}A_1^{\circ 2})\}\right]}{X_1^L\Delta^{\circ}H_1A_1^{\circ} + (1 - X_1^L)\Delta^{\circ}H_{\circ}\exp\{\frac{\Delta^{\circ}G_{\circ}}{RT_{\circ}^2} - \frac{X_1^{L\,2}}{2}(\epsilon_{11}^L - \epsilon_{11}^{\gamma}A_1^{\circ 2})\}}$$

for which

$$A_n^{\circ} = \frac{\exp\{\frac{\Delta^{\circ}G_n}{RT_{\circ}} + \epsilon_{1n}^L.X_1^L\}}{1 + \epsilon_{1n}^{\gamma}X_1^L\exp\{\frac{\Delta^{\circ}G_1}{RT_{\circ}}\}}$$

where $n = 1$ or i (Kirkaldy *et al.*, 1978).

$\Delta^\circ H_\circ$ and $\Delta^\circ H_1$ are the standard molar enthalpy changes corresponding to $\Delta^\circ G_\circ$ and $\Delta^\circ G_1$ respectively.

This was the relationship used for the determination of the Fe-C-X(i) multicomponent equilibrium phase diagram. The solute elements for which the program has been written are those that might commonly be found in low-alloy steels, (Mn, Si, Ni, Cr, Mo, and Cu), although, if the relevant free energy changes per unit of solute dissolving ($\Delta^\circ G$) and the interaction parameters (ϵ) are known, ΔT can in principle be calculated for any alloy.

4.4 PREDICTION OF AE3 TEMPERATURE

The overall intention of this and other current research is to be able to predict the mechanical properties of multipass welds. This requires a detailed knowledge of the thermal history of the weld, and necessarily the transformation temperatures of the steels. In welding, the Ae_3 temperature which has a considerable influence on, *inter alia*, the relative volume fractions of the phases present in the as-welded microstructure, and the size of the reaustenitised region in multipass welds. Therefore, as a first step, a program was written to allow the Ae_3 temperature to be predicted, using the method described. A series of modifications were incorporated into it as follows:

- The program had been used for Mn, Si, Ni, Cr, Mo and Cu additions (Baganis and Kirkaldy, 1978). In addition, the elements for Nb, Co, V, and W were included, using further data given by Kirkaldy *et al.* (1978).

- Ae_3 values for $T_\circ$ were formulated into a subroutine using accurate values derived from equations due to Bhadeshia and Edmonds (1980) giving $T_\circ$ down to 200°C. Extrapolating the Ae_3 in this manner would be potentially very useful, allowing, for example, growth rate kinetics to be calculated at temperatures well below the eutectoid temperature (Bhadeshia, 1985a).

- Although, data were provided for values for the standard Gibbs free energy change accompanying the α/γ transformation in pure iron (Harvig, 1978), $\Delta^\circ G_\circ^{\alpha\rightarrow\gamma}$, since a long-term aim was to extrapolate the Ae_3 to lower temperatures, the data due to Kaufman *et al.* (1963), which gives values down to 0K, and which are known to be reliable over the entire temperature range of

interest (Bhadeshia, 1985b) were used. $\Delta^\circ G_\circ^{\alpha\rightarrow\gamma}$ was represented by curve-fitting values from Table 3 of Kaufman *et al.* (1963), and later corrected values for $\Delta^\circ G_\circ^{\alpha\rightarrow\gamma}$(T> 1183) from Kaufman and Bernstein (1970).

- Values for $\Delta^\circ H_\circ^{\alpha\rightarrow\gamma}$ were obtained from work due to Kaufman *et al.* (1963). For temperatures below 1183K, the tabulated data were interpolated using cubic splines (Hayes, 1974).

In applying Eqn. 4.11 to the calculation of the Ae_3, Baganis and Kirkaldy (1978) had taken ϵ_{11}^{α} as taken zero. They argued that the error introduced is negligible, since the interaction parameter is multiplied only by the very low concentration of carbon in ferrite. This assumption can be assessed quantitatively. Figure 4.3 shows the carbon sublattice in a crystal of α-Fe. The b.c.c. unit cell contains two iron atoms and six carbon sites. (This ignores tetrahedral sites, but the probability of their occupation is rather low). From Figure 4.1, the maximum solubility of carbon in δ-iron is 0.09 wt% = 0.417 at%. Therefore, there are (99.6/0.417) = 239 iron atoms for every carbon atom, or there is one carbon atom for every 119 unit cells, so that, even at saturation, the probability of two carbon atoms even being in the same unit cell is only 0.004. Thus, their assumption seems justified and was adopted.

Since all the thermodynamic functions used were dependent on temperature, ΔT cannot be obtained from a single application of Eqn. 4.11, but has to be deduced iteratively. For this purpose, a loop was included in the program. Initially, T was set as $T_\circ$, and a trial value of ΔT was calculated. Then, the program was rerun with $T = (T + \Delta T)$. This procedure being repeated until the value of T changed by less than 1° in successive iterations (typically 5 times). A listout of the program is given in Appendix 1. Results for all the alloying elements were drawn up and checked for correspondence with data from Fe-X binary phase diagrams compiled by Kubaschewski (1982), and overall agreement was excellent. However, discrepancies were observed with the Fe-Mn, Fe-Ni, and Fe-Nb systems, and these are discussed here.

- **Fe-Mn:** As Baganis and Kirkaldy (1978) also found, a systematic discrepancy was observed between experimental and calculated values for the Fe-Mn system, attributable to errors in $\Delta^\circ G_{\mathrm{Mn}}^{\alpha\rightarrow\gamma}$. Instead, data were used due to Gilmour *et al.* (1972), who calculated $\Delta^\circ G_{\mathrm{Mn}}^{\alpha\rightarrow\gamma}$ between 700 and 850°C using experimental

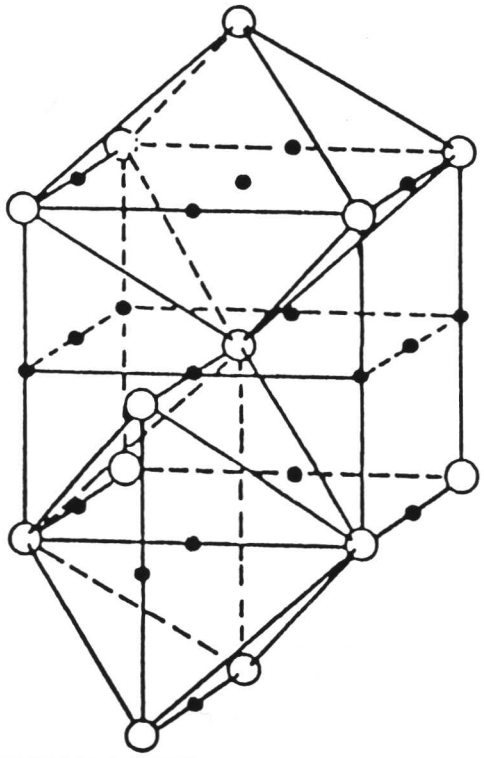

Figure 4.3: Location of the octahedral interstices [•] in a b.c.c. crystal. (After Cohen, M. (1962), *Trans. AIME*, **224**, 645).

results on the Fe-C-Mn system. In their work, $\Delta^\circ G_{\mathrm{Mn}}^{\alpha\rightarrow\gamma}$ was found as a function of temperature from a knowledge of the activities, and molar concentrations, of manganese in austenite and ferrite at equilibrium to give

$$\Delta^\circ G_{\mathrm{Mn}}^{\alpha\rightarrow\gamma} = 25.57\mathrm{T/K} - 32640 \text{ J/mol} \tag{4.12}$$

- **Fe-Ni:** Kirkaldy *et al.* (1978) postulated that errors in predicting the Ae_3 at lower carbon contents (higher temperatures) might be due in part to an error in $\Delta^\circ G_{\mathrm{Ni}}^{\alpha\rightarrow\gamma}$. Sharma and Kirkaldy (1973), whose data had been used by Kirkaldy *et al.* (1978), give

$$\Delta^\circ G_{\mathrm{Ni}}^{\alpha\rightarrow\gamma} = -1.90 \times 10^4 + 13.5T \text{ J/mol} \tag{4.13}$$

A new value for $\Delta^\circ G_{\mathrm{Ni}}^{\alpha\rightarrow\gamma}$ was calculated for the present work using the value for $\Delta^\circ G_{\mathrm{Ni}}^{\gamma\rightarrow L}$ given by Uhrenius. (Uhrenius, 1978). Thus, since these quantities are additive

$$\begin{aligned}
\Delta^\circ G_{\mathrm{Ni}}^{\alpha\rightarrow\gamma} &= \Delta^\circ G_{\mathrm{Ni}}^{\alpha\rightarrow L} - \Delta^\circ G_{\mathrm{Ni}}^{\gamma\rightarrow L} \\
\Delta^\circ G_{\mathrm{Ni}}^{\alpha\rightarrow L} &= 8.88 \times 10^4 - 1.59T \text{ J/mol (Kirkaldy } \textit{et al.}\text{, 1978)} \\
\Delta^\circ G_{\mathrm{Ni}}^{\gamma\rightarrow L} &= 1.46 \times 10^4 \text{ J/mol (Uhrenius, 1978)}
\end{aligned}$$

which gives

$$\Delta^\circ G_{\mathrm{Ni}}^{\alpha\rightarrow\gamma} \approx -2.35 \times 10^4 - 1.6T \text{ J/mol} \tag{4.14}$$

These changes made for a substantial improvement in the description of the Fe-Ni system.

- **Fe-Nb:** A large deviation from the α/γ phase boundary was found due to an error in $\Delta^\circ G_{\mathrm{Nb}}^{\alpha\rightarrow\gamma}$. Kirkaldy *et al.* (1978) give

$$\Delta^\circ G_{\mathrm{Nb}}^{\alpha\rightarrow\gamma} = 60.0 - 5.4 \times 10^{-3}T \text{ J/mol} \tag{4.15}$$

a)

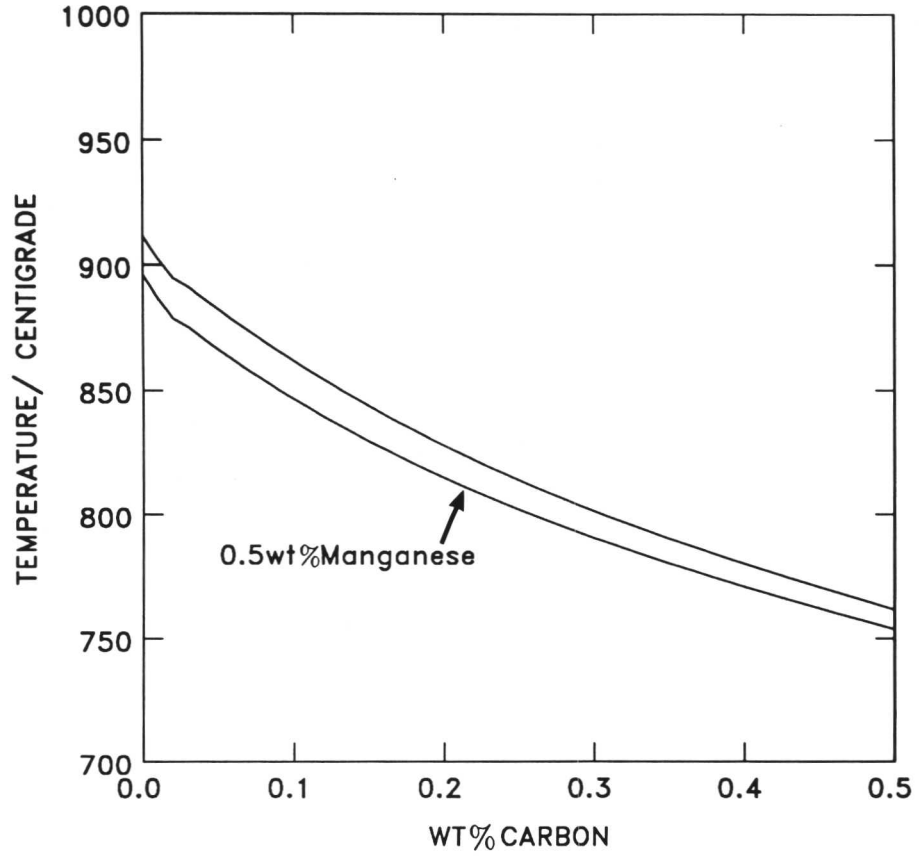

b)

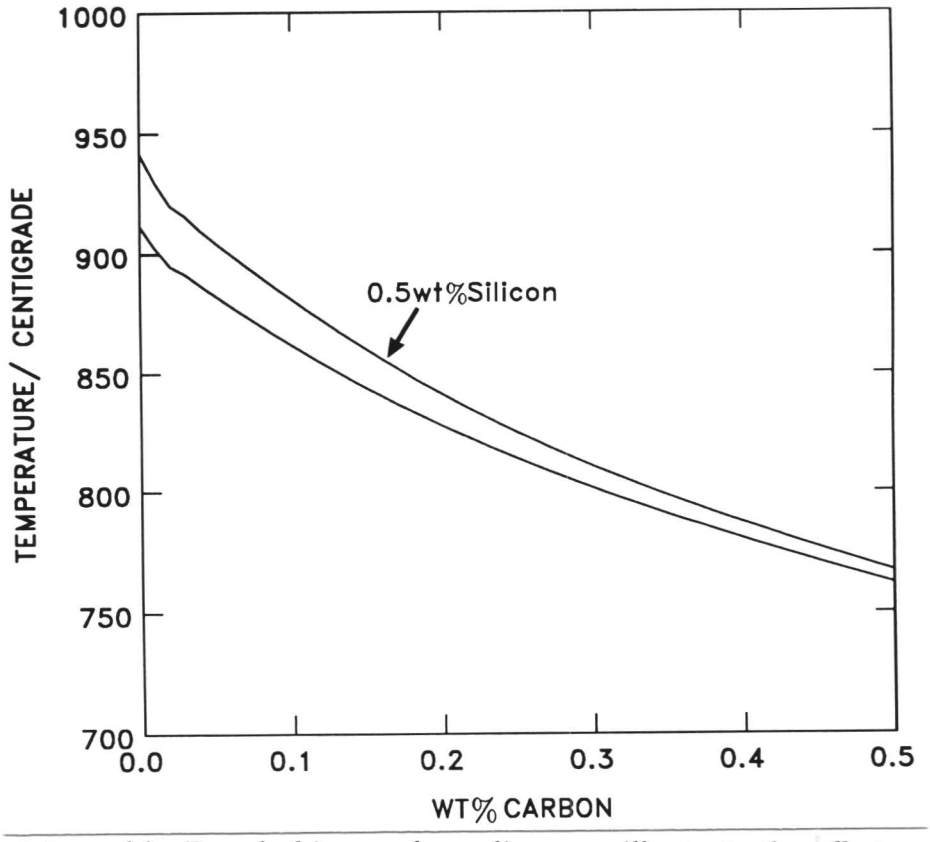

Figures 4.4a and b: Pseudo-binary phase diagrams illustrate the effect on the Ae_3 temperature of adding 0.5 wt% of a) manganese and b) silicon to binary iron-carbon.

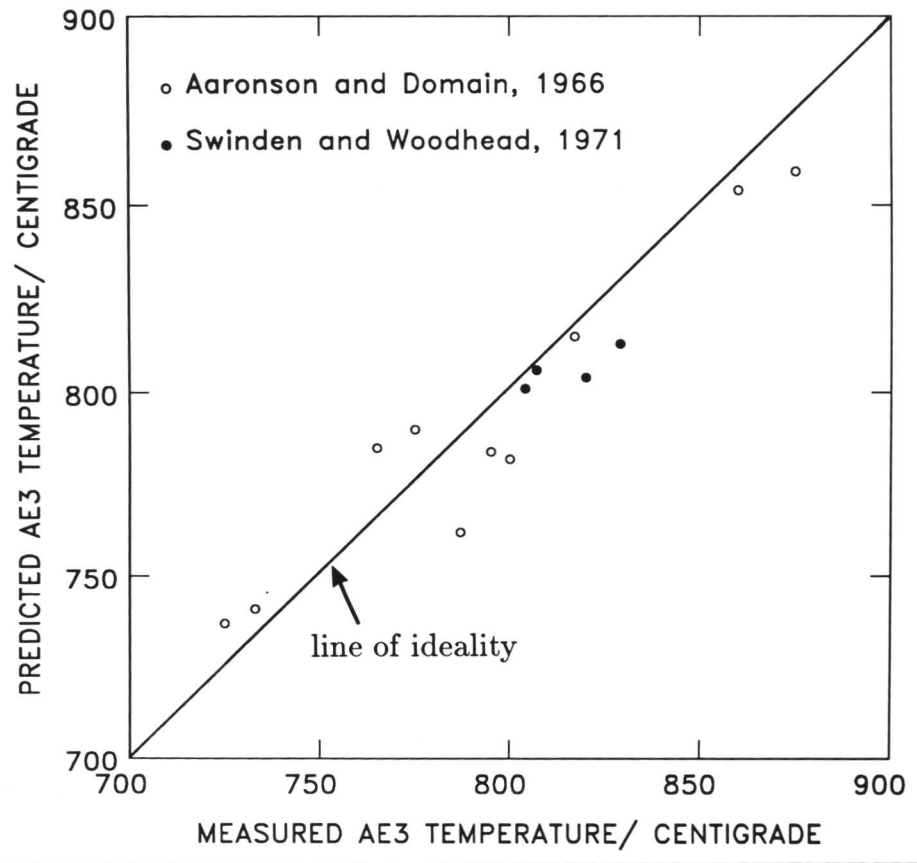

Figure 4.5: Comparison of predicted and measured values for the Ae_3 temperature for a variety of steels.

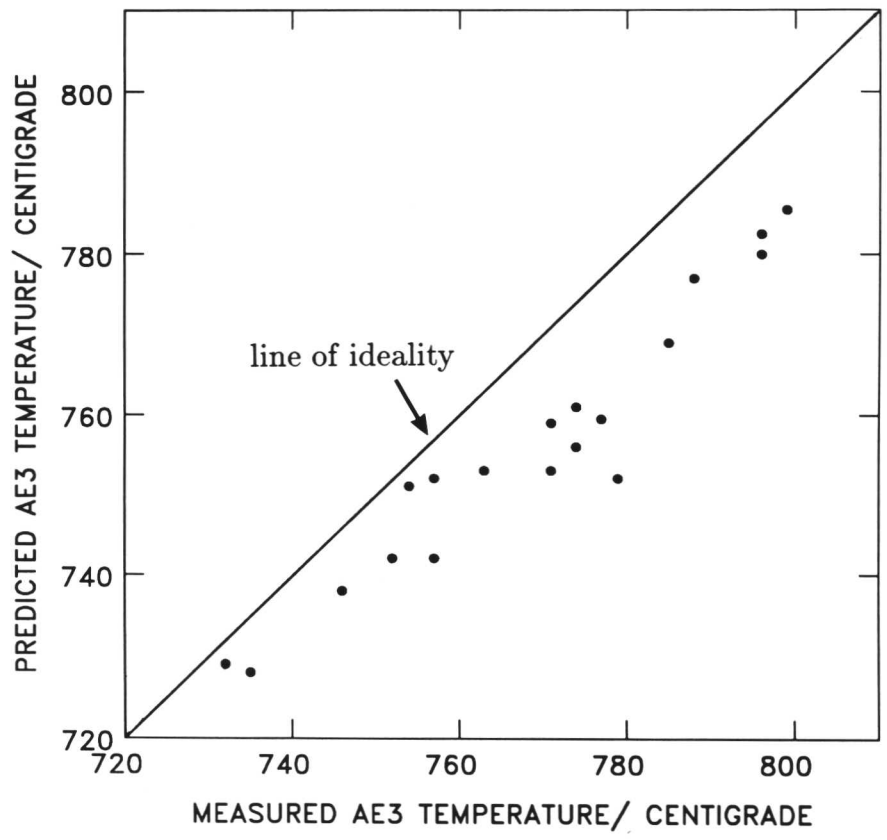

Figure 4.6: Experimental and calculated values for the Ae_3, using experimental data due to Grange (1961).

the standard error being less than ±10°C. Data were also taken from Grange (1961) consisting of an analysis of nineteen medium carbon low-alloy steels of commercial purity. Grange identified the Ae_3 temperature as the temperature at which the last trace of *ferrite* transformed to austenite on prolonged isothermal heating. This work, as with dilatometry on heating, would tend to yield higher than true equilibrium values. This concurs with the results obtained in Figure 4.6, the mean apparent overshoot of the experimental results obtained being approximately 8°C.

4.5 PREDICTION OF PERITECTIC REGION

4.5.1 Liquidus Temperature

Over recent years it has become apparent that the mode of solidification is a determining factor in the subsequent development of the weld metal microstructure (Watanabe, 1975; Cochrane, 1983). However, to attempt to model the former would require a knowledge of the steel's solidification behaviour. Although, Eqn. 4.11 had been applied widely to the prediction of the Ae_3 temperature, the accuracy of the equation at predicting the liquidus and other peritectic temperatures of low-alloy multicomponent steels does not seem to have been verified. Kirkaldy and Baganis did compute the peritectic part of the phase diagram for several ternary alloys, but their calculations do not appear to have been compared against experimental data.

At the outset of this work, an attempt was made to avoid some of the mathematical assumptions made by Kirkaldy *et al.* (1978) in deriving Eqn. 4.11, [see Appendix I of Kirkaldy *et al.*(1978)]. To do this, the three equations which had been combined to derive Eqn. 4.11 were solved individually. The first two equations quantitatively define X_1^γ and X_i^γ $(i = 2 \rightarrow 11)$ as a function of alloy content, thus

$$X_1^\gamma \exp(\epsilon_{11}^\gamma X_1^\gamma) = X_1^L \exp\left(\frac{\Delta^\circ G_1}{RT_\circ} - \frac{\Delta^\circ H_1 \Delta T}{RT_\circ(T_\circ + \Delta T)} + \epsilon_{11}^L X_1^L\right) \quad (4.18)$$

$$\text{and} \quad X_i^\gamma \exp(\epsilon_{1i}^\gamma X_i^\gamma) = X_i^L \exp\{\frac{\Delta^\circ G_i}{RT_\circ} + \epsilon_{1i}^L X_i^L\} \quad (4.19)$$

Then, the deviation from the Fe-C liquidus boundary, ΔT, is obtained by solving for X_1^γ and X_i^γ, and substituting into Eqn. 4.20:

$$\frac{\Delta^\circ G_o}{RT_\circ} - \frac{\Delta^\circ H_\circ \Delta T}{RT_\circ(T+\Delta T)}$$

$$- \ln|1 - X_1^\gamma - \sum_{i=2}^{n} X_i^\gamma| + \ln|1 - X_1^L - \sum_{i=2}^{n} X_i^L|$$

$$+ \frac{\epsilon_{11}^\gamma}{2}(X_1^\gamma)^2 - X_1^\gamma \sum_{i=2}^{n} \epsilon_{1i}^\gamma X_i^\gamma + \frac{\epsilon_{11}^L}{2}(X_1^L)^2 - X_1^L \sum_{i=2}^{n} \epsilon_{1i}^L X_i^L = 0 \qquad (4.20)$$

In fact, it was soon found that these equations gave almost the same answers as those calculated using Eqn. 4.11, and because this method was much more complicated, it was abandoned.

Most of the data required were already found in Kirkaldy *et al.* (1978).† However, several phase boundaries on the binary phase diagram were not included in that analysis; these were the ferrite and austenite solida, and the $\delta/\delta+\gamma$ line. Also, the equation given in Kirkaldy *et al.* (1978) for $T_\circ$ for the austenite liquidus as a function of carbon due to Benz and Elliott (1961) did not appear to match

† The data in Kirkaldy *et al.* (1978) contain the following errata:

1. $\Delta^\circ G_{\rm Mn}^{\alpha\rightarrow\gamma} = -26650 + 42.69T - 0.017T^2$ cal/mol, not $0.17T^2$.
2. $\Delta^\circ G_{\rm Mn}^{\gamma\rightarrow\delta} = 430 - 0.305T$ cal/mol, not 650.
3. $\Delta^\circ G_{\rm Mn}^{\alpha\rightarrow\gamma} = 3500 - 2.308T$ cal/mol, not 3100.
4. Table III should be headed $\Delta^\circ G_i^{\gamma\rightarrow L}$, not $\Delta G_i^{\alpha\rightarrow L}$.
5. $\Delta^\circ H_1^{\gamma\rightarrow L} = -5360$ cal/mol, not -5630.
6. $T_\circ^{\gamma\rightarrow\gamma+\alpha} = 1185 - 150.3\text{wt\%C} + 216(0.865\text{wt\%C})^{4.26}$ K, not 1115.

Equation 1, and in Appendix I, Eqns. 2, 14, 17, 18, 21, and 22 are also published incorrectly, and the reader is referred to this text, and to Baganis and Kirkaldy (1978). In addition, in Tables I, II, and III, the standard state superscripts are omitted.

published A.S.M. data (Figure 4.1), and a new curve was calculated. From the Fe-C equilibrium phase diagram the lines were respectively calculated to be

$$T_\circ^{\delta\rightarrow\delta+L} = 1809 - 201.3(\text{wt\%C})\ \text{K} - 2949(\text{wt\%C})\ \text{K} \quad (4.21a)$$

$$T_\circ^{\gamma\rightarrow\gamma+L} = 1793 - 146.7(\text{wt\%C}) - 16.74(\text{wt\%C})^2\ \text{K} \quad (4.21b)$$

$$T_\circ^{\gamma+\delta\rightarrow\delta} = 1666 + 1122(\text{wt\%C})\ \text{K} \quad (4.21c)$$

$$\text{and} \quad T_\circ^{\gamma+L\rightarrow L} = 1783 - 164.0(\text{wt\%C}) - 7.869(\text{wt\%C})^2\ \text{K} \quad (4.21d)$$

In order to find out if any data values were suspect, the carbon contents, X_1^L was set to zero so that dilute binary phase diagrams were generated for each element. In this way ΔT for each solute element could be checked. Although, general agreement was excellent, a systematic discrepancy was found for the Fe-Mn system, and in this work $\Delta^\circ G_{\text{Mn}}^{\alpha\rightarrow L}$ has been estimated from values for $\Delta^\circ G_{\text{Mn}}^{\alpha\rightarrow\delta}$ and $\Delta^\circ G_{\text{Mn}}^{\gamma\rightarrow L}$. Kirkaldy *et al.* (1978) give

$$\Delta^\circ G_{\text{Mn}}^{\gamma\rightarrow\delta} = 2.72\times10^3 - 1.28T\ \text{J/mol}$$

$$\text{and} \quad \Delta^\circ G_{\text{Mn}}^{\gamma\rightarrow L} = 1.20\times10^4 - 8.50T\ \text{J/mol} \quad (4.22)$$

These two functions are then combined to give

$$\Delta^\circ G_{\text{Mn}}^{\alpha\rightarrow L} = \Delta^\circ G_{\text{Mn}}^{\delta\rightarrow\gamma} + \Delta^\circ G_{\text{Mn}}^{\gamma\rightarrow L}$$

$$= 9.25\times10^3 - 7.22T\ \text{J/mol} \quad (4.23)$$

A listout of the peritectic program is given in Appendix 3. As with the Ae_3 program, a temperature loop was included in the program to increase the accuracy of the final result.

In order to assess the overall accuracy of the program, experimental data were taken from Jernkontoret (1977), in which values for the liquida, solida, and solidification ranges of a wide range of steels have been measured by differential thermal

Steel	Composition/wt%								
No.	C	Mn	Si	Ni	Cr	Mo	Cu	V	Nb
201	0.11	1.25	0.12	0.03	0.06	0.07	0.07		
202	0.12	1.53	0.27	0.03	0.02	0.03	0.05		
203	0.18	1.26	0.44	0.02	0.01	0.06	0.02		0.03
204	0.19	1.42	0.40	0.13	0.07	0.02	0.08		
205	0.36	0.58	0.27	0.05	0.08	0.02	0.12		
206	0.69	0.72	0.23	0.02	0.02	0.01	0.03		
207	1.01	0.46	0.25	0.03	0.02	0.02	0.03		
209	0.20	0.90	0.25	1.05	0.81	0.06	0.07	0.02	
211	0.29	0.62	0.21	0.15	1.11	0.21	0.04	0.04	
213	0.35	0.67	0.24	0.05	0.92	0.19	0.07	0.02	
214	0.52	0.85	0.22	0.07	1.07	0.07	0.04	0.14	
216	1.01	0.33	0.23	0.02	1.55	0.01	0.04	0.04	
1	0.30	0.13	0.10	0.05	0.30	0.024			
2	0.48	0.04	0.06	0.015	0.08	0.016			
3	0.66	0.04	0.31	0.015	0.04	0.007			
4	0.81	0.04	0.41	0.02	0.03	0.012			
5	0.58	<0.02	0.99	<0.02	0.03	<0.02			
6	0.89	<0.02	0.43	<0.02	0.02	<0.02			
7	1.20	<0.02	0.53	0.03	<0.02	<0.02			
8	1.48	<0.02	0.55	0.04	0.02	<0.02			
25	0.004	0.14	0.11		0.03				
26	0.001	0.02	0.32	0.02	0.04	0.005			

Table 4.1: Compositions in wt% of the low-alloy multicomponent steels analysed. Data are taken from Jernkontoret (1977) [Steels 201 → 216], and Howe (1988) [Steels 1 → 26].

No.	Primary Solidification Mode	Measured Liquidus Temperature/ °C	Predicted Liquidus Temperature/ °C
201	Ferritic	1515	1523
202	"	1514	1520
203	"	1507	1516
204	"	1506	1514
205	"	1501	1507
206	Austenitic	1474	1479
207	"	1459	1458
209	Ferritic	1503	1505
211	"	1503	1508
213	"	1495	1504
214	Austenitic	1483	1485
216	"	1451	1454
1	Ferritic	1505	1516
2	"	1470	1500
3	Austenitic	1476	1482
4	"	1464	1470
5	"	1472	1477
6	"	1456	1465
7	"	1437	1441
8	"	1408	1419
25	Ferritic	1529	1534
26	"	1530	1532

Table 4.2: Measured and predicted values for the liquidus temperatures of 22 low-alloy steels.

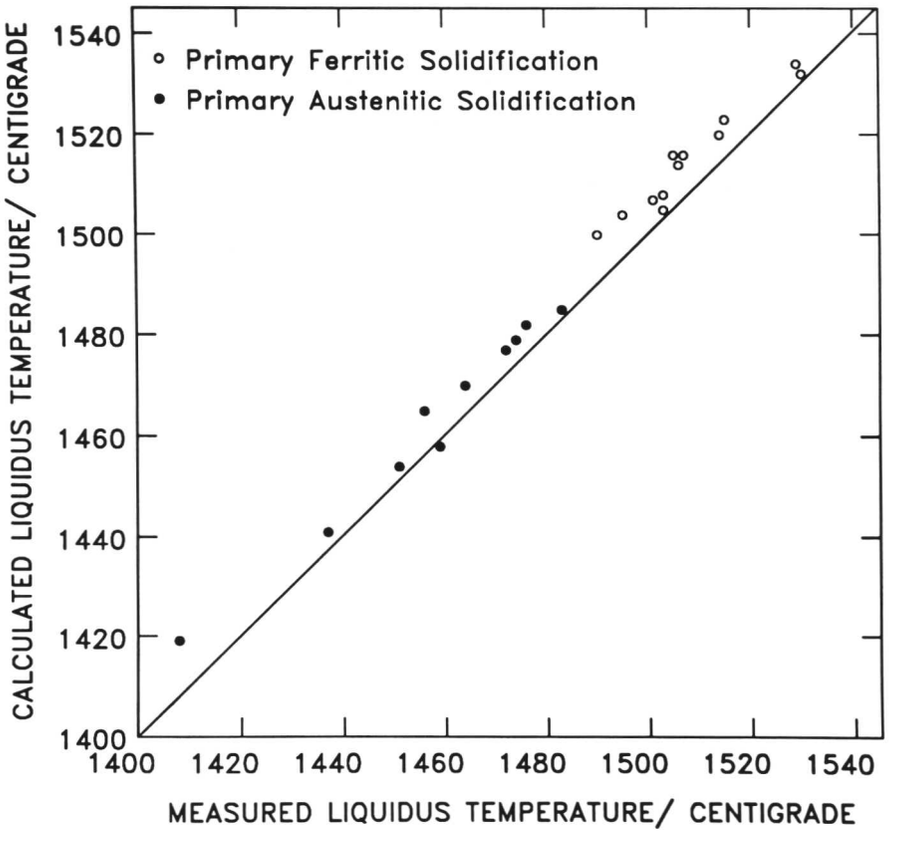

Figure 4.7: Predicted and measured liquidus temperatures for twenty-two low-alloy steels for primary ferrite and primary austenite solidification. The data are taken from Jernkontoret (1977), and Howe (1988).

analysis at a variety of cooling rates. In addition, newly published experimental data due to Howe (1988), giving the liquidus temperatures of a wide range of steels, were used. The compositions of the steels for which $\sum_{i=2}^{n} X \leqslant 6$ wt% are given in Table 4.1. For this analysis, data from Jernkontoret obtained at the slowest cooling rates (0.1°C/s) were used, since these are expected to be closest to equilibrium. Experimental and calculated values for the liquidus temperatures of the steels given in Table 4.1, are listed in Table 4.2 and plotted in Figure 4.7. It can be seen that agreement is excellent, and actually better than that achieved for the Ae_3, the slight overestimation for the liquidus being conceivably attributable to the measurements being made under continuous cooling conditions.

4.5.2 Solidification as Primary Austenite

The small differences in Gibbs free energy between various equilibria in the Fe-C system means that metastable equilibria should also be considered, since metastable phases may be kinetically favoured. Depending upon the composition and cooling conditions, steels may solidify directly as austenite or ferrite, and, in general, the close proximity of the liquidus surfaces of these two phases means that metastable formation of one phase may occur when equilibrium data indicate that the other phase is the stable one (Fredriksson and Hellner, 1974; Fredriksson, 1976). One particular advantage of using thermochemical calculations is that the $\gamma/\gamma + L$ phase boundary is readily calculable. High cooling rates can obviate nucleation of the δ phase above the peritectic temperature, so that solidification then proceeds according to the austenite-cementite system. Since solute elements have different solubilities and diffusion rates in ferrite and in austenite, segregation is directly influenced by the form of the primary precipitation. Specifically, the diffusion rate of substitutional elements in ferrite is two orders of magnitude greater than in austenite, and consequently segregation during a ferritic solidification process is much smaller than during an austenitic one (Edvardsson *et al.*, 1976). This behaviour has profound significance in welding since solidification as austenite will not only result in differences in solute segregation, but also in the distribution of the inclusions in the weld with respect to the phases that subsequently form.

Figure 4.8 shows the austenite-graphite and austenite-cementite phase diagram, where the stable boundaries are indicated by full lines, those of the austenite-cementite equilibria by dashed lines. This metastable system has been constructed in the program by extrapolating the austenite solidus and austenite liquidus. It

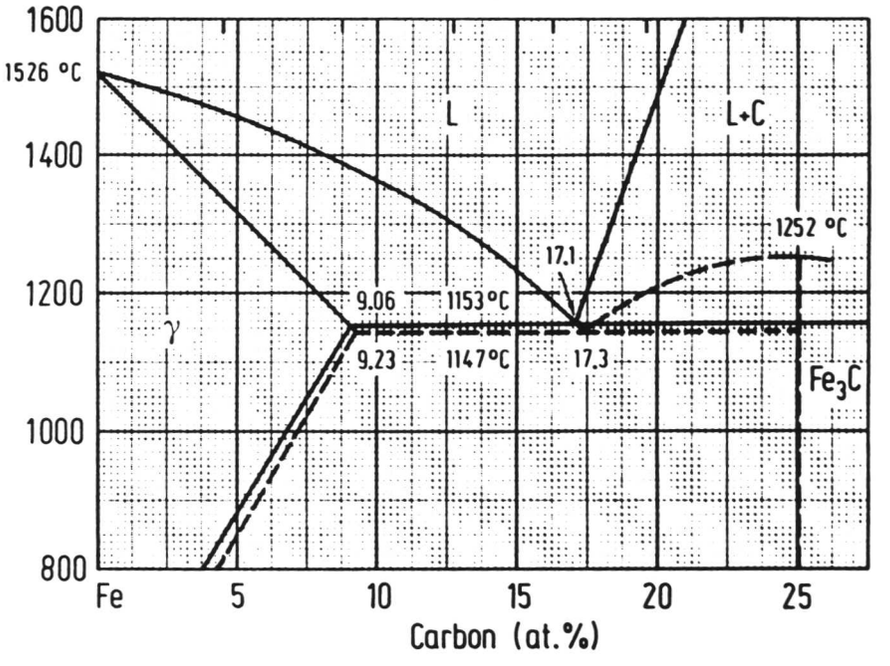

Figure 4.8: Fe-C equilibria of austenite with graphite and cementite. (After O. Kubaschewski, "Iron-Binary Phase Diagrams" (1982), Springer-Verlag, Berlin, FDR, 23-25).

can be seen that the melting point of γ-Fe is only some 10K lower than the melting point of δ-Fe.

4.5.3 Prediction of Solidification Ranges

Solidification of an alloy with a finite freezing range can allow the formation of an inhomogeneous solid, and the amount of eventual segregation may be directly related to the solidification range of the alloy. It was, therefore, crucial to check the accuracy of the program at predicting the solidus temperatures and solidification ranges of the steels analysed. For steels 201 and 202, which respectively contain 0.11 and 0.12 wt%C, and which solidify through the peritectic as δ-ferrite, the δ solidus was estimated, to a first approximation, by extrapolation of the δ solidus line. For the other steels, it was calculated from the austenite solidus. Table 4.3 lists measured and predicted values of the solidus temperatures and solidification ranges for the Jernkontoret steels. These data are plotted in Figures 4.9 and 4.10 respectively. As with the liquidus, it can be seen that the thermodynamic algorithm is an excellent predictor of both the solidus temperature and the solidification range of the steels.

	Solidus Temperature		Solidification Range	
No.	Measured/ °C	Predicted/ °C	Measured/ °C	Predicted/ °C
201	1455	1471	60	52
202	1460	1460	54	60
203	1460	1470	47	46
204	1460	1467	46	47
205	1440	1442	61	65
206	1370	1383	104	96
207	1340	1321	119	137
209	1445	1459	58	46
211	1450	1450	53	58
213	1425	1440	70	64
214	1400	1410	83	75
216	1300	1318	151	136

Table 4.3: Calculated and measured solida and solidification ranges for the steels analysed.

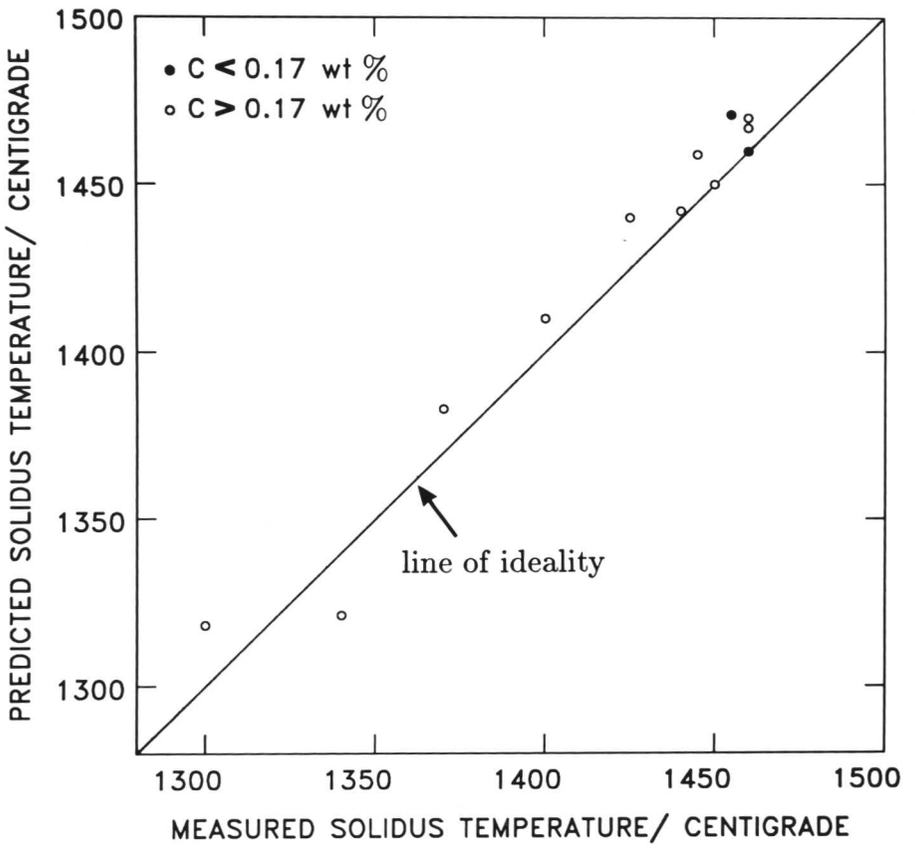

Figure 4.9: Experimental and calculated values for the solidus temperature of a range of twelve low-alloy multicomponent steels. The data are due to Jernkontoret (1977). (0.17wt% carbon corresponds to the peritectic point on the binary Fe-C equilibrium phase diagram, and thus indicates a change in solidification mode for the alloys).

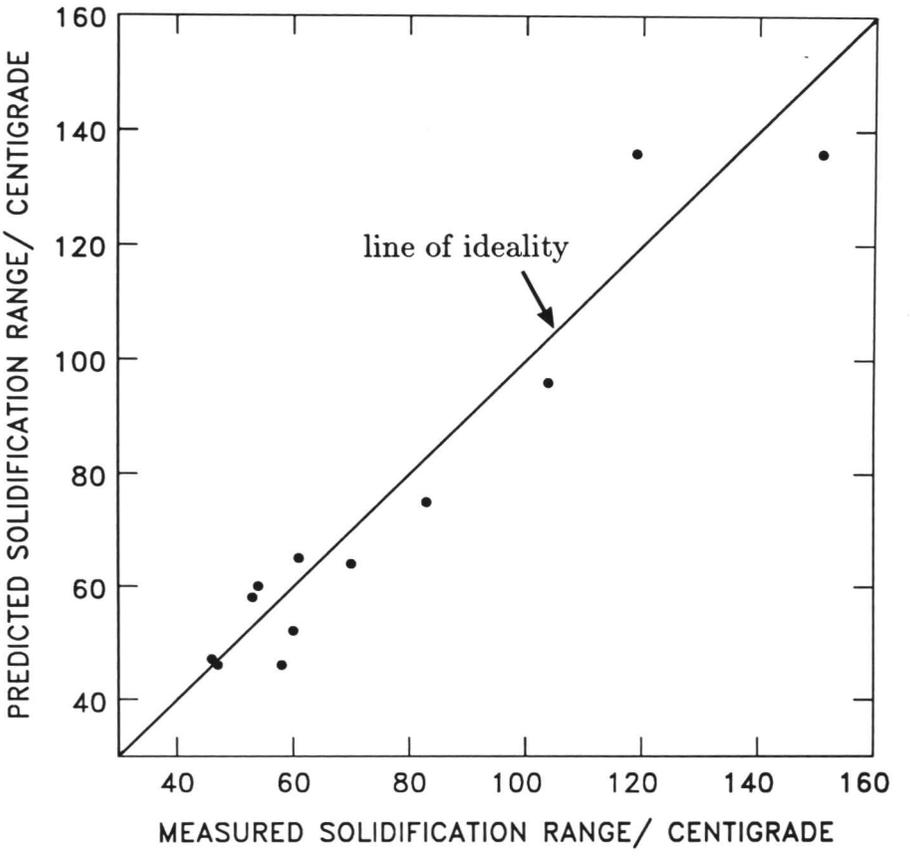

Figure 4.10: Experimental and calculated values for the solidification range of twelve low-alloy steels given in Table 4.1.

Figures 4.11a and b show the entire peritectic region drawn using the computer model. The diagrams show two constant sections through the Fe-C-Mn and Fe-C-Cr phase diagram for 0 and 1.0 wt% manganese, and 0 and 2.0 wt% chromium. Although, the exact composition of the phases in microscopic equilibrium cannot be predicted from a pseudo-binary diagram, trends in compositional change can. Depression of the peritectic and Ae_3 temperatures can be seen. Note also stabilization of the austenite phase field and a concomitant contraction of the δ phase field for manganese, and the corresponding expansion of the δ field and contraction of the austenite field when chromium is present.

4.6 CALCULATION OF PARTITION COEFFICIENTS

The partition coefficient of a solute element is a characteristic value showing the degree of microsegregation of an element in an alloy system. To determine the equilibrium partition coefficients of solute elements for multicomponent systems entails time-consuming experiments. Therefore, the application of thermodynamic calculations to the determination of partition coefficients is a logical step, particularly since, for a dilute solution containing small amounts of alloying elements, the contribution from the interaction among the elements to the partition coefficient between δ-ferrite or austenite and liquid iron is negligible (Kagawa *et al.*, 1985). Since the cooling rates encountered in welding are quite high, it can be assumed that segregation arising during solidification is not influenced by subsequent diffusion during cooling from the liquidus (Gretoft *et al.*, 1986). By considering the steel at a temperature at which both the ferrite and austenite are in equilibrium, the proportions of these two phases, and their composition (*i.e.* the partition of the alloy elements) can also be calculated. The partition coefficient of a given solute element is determined using the relationship given in Eqn. 4.11. For example, for the γ/L transformation,

$$X_i = X_i^L A_i \tag{4.24}$$

$$\text{where} \quad A_i = \frac{\exp\left(\frac{\Delta^\circ G_i}{RT^\circ} + \epsilon_{1i}^L X_1^L\right)}{1 + \epsilon_{1i}^\gamma X_1^L \exp\frac{\Delta^\circ G_1}{RT^\circ}}$$

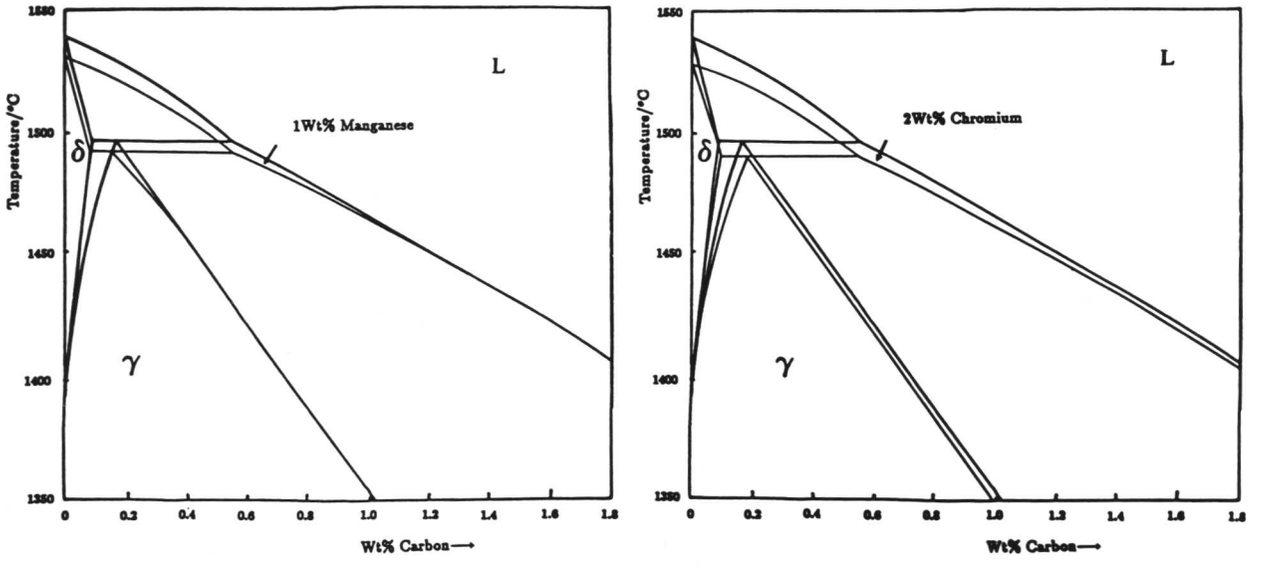

Figures 4.11a and b: Fe-C-Mn and Fe-C-Cr phase diagrams. The diagrams were constructed using points generated by the computer model. (Note: for simplicity, the three-phase peritectic region has been kept as a straight line).

a)

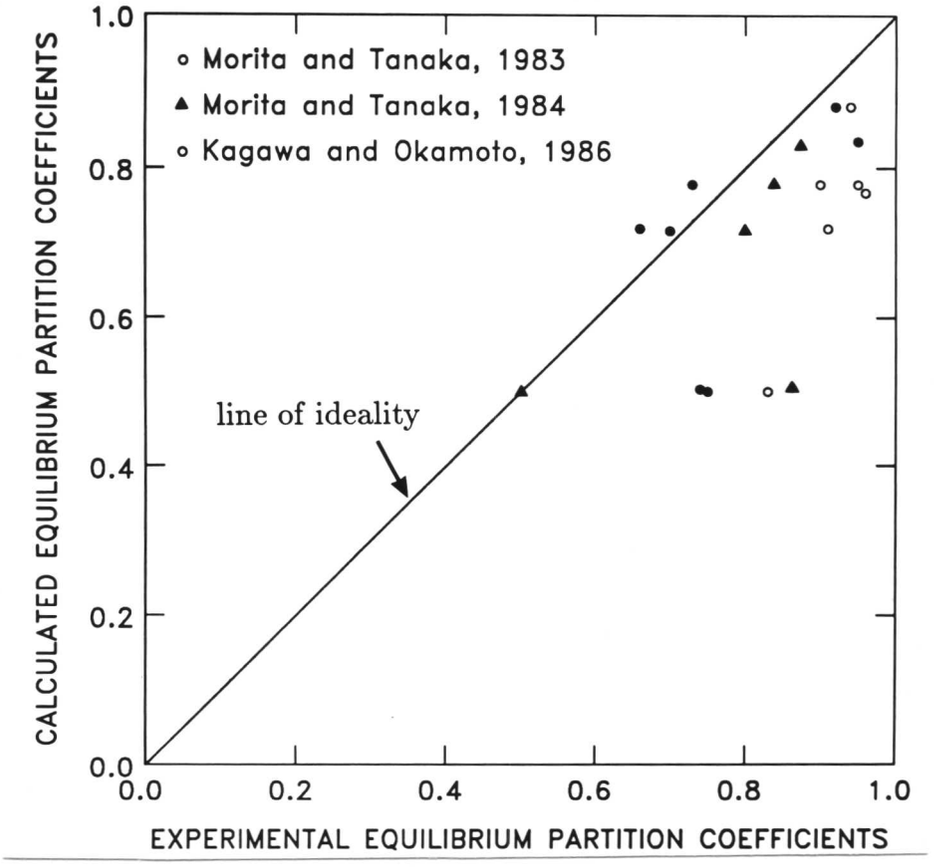

b)

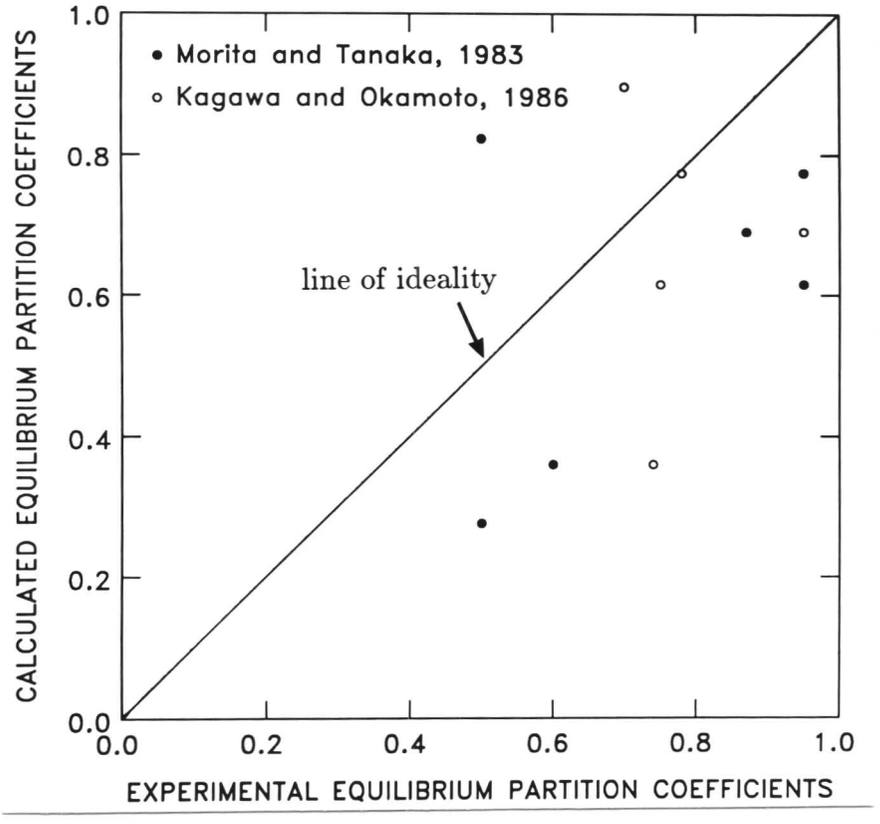

Figures 4.12a and b: Calculated and experimental values for the equilibrium partition coefficients of solute elements for a) δ-ferrite and liquid iron, and b) austenite and liquid iron. Lines are lines of ideality.

4.7 SUMMARY

Standard free energy changes and activity data for iron and its binary and ternary alloys have ben used to evaluate the general linear series (Wagner) expansion of the activity coefficient, and these have themselves been used to generate an accurate thermodynamic determination of equilibrium multicomponent Fe-C-X transformation temperatures. A computer program has been written which accurately describes the influence of low concentrations of alloying elements on the Ae_3 equilibrium temperature of low-alloy steels containing for up to 1.8 wt%C. Using the method due to Baganis and Kirkaldy (1978), the phase boundary is calculated using empirical data to estimate the Gibbs free energy of the participating phases in the multicomponent system, and the resultant deviation of the phase boundary from that of the binary Fe-C system is then found. New elements (V, Nb, W, Co) have been incorporated to the program, and revised values for $\Delta^\circ G_\circ$, $\Delta^\circ H_\circ$, and $T_\circ$ have been used. In addition, discrepancies with the Fe-Mn, Fe-Ni, and Fe-Nb systems have been resolved. The program has been shown to be valid for significant additions of Mn, Si, Ni, Cr, Mo, Cu, V, Nb, W and Co.

The peritectic region of the phase diagram has been calculated, with each phase boundary being treated individually, and for the first time its accuracy evaluated. Results obtained by calculation have been compared with experimental data for the liquida and solida of a range of low-alloy multicomponent steels, and found to be in extremely good agreement. A good ability to predict the solidification range, which strongly influences the amount of solute segregation, was also obtained. Finally, an attempt has been made to estimate the amount of partitioning for alloying elements between δ- and liquid iron, and between austenite and liquid iron, and agreement with observed results was fair. This model has been shown to accurately predict the modifications to the Fe-Fe_3C phase diagram of any given set of alloying elements, in the following range: C$\leqslant$ 1.8wt%, Mn$<$ 3.0%, Ni$<$ 2.5%, Cr$<$ 2.5%, Co$<$ 2%, Mo$<$ 1.5%, rest (including Si)$\leqslant$ 1.0%. This covers the largest proportion of steels used in welding fabrication.

The practical limitations of the program arise from two sources, namely, the limitations of the theory itself, in particular the inability to account for solute-solute interactions, since it is only strictly correct for infinitely dilute solutions, and inadequate experimental data for the pure binary systems with iron as one component. It is anticipated that these source data will be refined as development

of the program continues.

REFERENCES

AARONSON, H. I. and DOMAIN, H. A. (1966), *Trans. AIME*, **236**, 781-796.

ANDREWS, K. W. (1956), *J.I.S.I.*, **184**, 414-427.

BAGANIS, E. and KIRKALDY, J. S. (1978), *Metall. Trans. A*, **9A**, (4), 495-501.

BENZ, M. G. and ELLIOTT, J. F. (1961), *Trans. AIME*, **221**, 323-331.

BHADESHIA, H. K. D. H. (1985a), *Prog. Mat. Sci.*, **29**, 321-386.

BHADESHIA, H. K. D. H. (1985b), *Mat. Sci. Tech.*, **1**, 497-504.

BHADESHIA, H. K. D. H. and EDMONDS, D. V. (1980), *Acta Metall.*, **28**, 1265-1273.

COCHRANE, R. C. (1983), *Weld. World*, **21**, 16–24.

COHEN, M. (1962), *Trans. AIME*, **224**, 638-656.

CRASKA, P. and McLELLAN, R. B. (1971), *Acta Metall.*, **19**, 1219-1225.

DARKEN, L. S. and GURRY, R. W. (1953), "Physical Chemistry of Metals", McGraw-Hill Book Co. Ltd., Kōgakusha, Tokyo, Japan, 404-405.

EDVARDSSON, T., FREDRIKSSON, H., and SVENSSON, I. (1976), *Met. Sci.*, **10**, (9), 298-306.

EROKIN, A. A., BALAUDIN, G. F., and KODOLOV, V. D., (1960) *Automat. Weld.*, **82**, 18–24.

FLEMINGS, M. C., POIRIER, D. R., BARONE, R. V., AND BRADY, H. D. (1970), *J.I.S.I.*, **208**, (4), 371-381.

FREDRIKSSON, H. (1976), *Met. Sci.*, **10**, (3), 77–86.

FREDRIKSSON, H. (1977), "Solidification and Casting of Metals", *[Proc. Conf.]*, Metals Society, London, U.K., 131–138.

FREDRIKSSON, H. and HELLNER, L. (1974), *Scand. J. Metall.*, **3**, 61-68.

FREDRIKSSON, H. and STJERNDAHL, J. (1982), *Met. Sci.*, **16**, (10), 575–585.

GILMOUR, J. B., PURDY, G. R., and KIRKALDY, J. S. (1972), *Metall. Trans.*, **3**, 1455-1464.

GRANGE, R. A. (1961), *Met. Prog.*, **79**, (4), 73-75.

GRETOFT, B., BHADESHIA, H. K. D. H., and SVENSSON, L-E. (1986), *Acta Stereol.*, **5**, (2), 365-371.

HANSEN, M. (1958), "The Constitution of Binary Alloys", McGraw Hill Book Co., New York, 676.

HARVIG, H. (1978), "The Iron-Carbon System in the Temperature Range 500-1150°C", *Jernkont. Ann.*, **155**, 157-161.

HAYES, J. G. (1974), *Bull. Inst. Maths. Applics.*, **10**, 142-152.

HILLERT, M. and STAFFANSSON, L.-I. (1976), *Metall. Trans. B*, **7B**, (6), 203-211

HONE, M., SUBRAMANIAN, S. V., and PURDY, G. R. (1969), *Can. Met. Quart.*, **8**, (3), 251-256.

HOWE, A. A. (1988), *Iron. and Steel.*, **15**, (3), 134-142.

HUDD, R. C., JONES, A., and KALE, M. N. (1971), *J.I.S.I.*, **209**, (2), 121-125.

JERNKONTORET (1977), "A Guide to the Solidification of Steels", Jernkontoret, Box 1721, S-11187 Stockholm, Sweden, 155-156.

KAGAWA, A., IWATA, K., NOFAL, A. A., and OKAMOTO, T. (1985), *Mat. Sci. Tech.*, **1**, 678-683.

KAGAWA, A. and OKAMOTO, T. (1986), *Ibid.*, **2**, (10), 997-1008.

KATTAMIS, T. Z. and FLEMINGS, M. C. (1965), *Trans. AIME*, **233**, 992-999.

KAUFMAN, L. and BERNSTEIN, H. (1970), "Computer Calculation of Phase Diagrams; with special reference to Refractory Metals", (Refractory Materials, Vol. 4), Academic Press, New York, 19.

KAUFMAN, L., CLOUGHERTY, E. V., and WEISS, R. J., *Acta Metall.*, **11**, (5), 323-335.

KIRKALDY, J. S., THOMSON, B.A., and BAGANIS, E. A., (1978) "Hardenability Concepts with Applications to Steel", *[Proc. Conf]*, Eds., D. V. Doane and J. S. Kirkaldy, *Met. Soc. AIME*, AIMMPE, Warrendale, PA 15086, U.S.A., 82–125.

KUBASCHEWSKI, Ortrud (1982), "IRON-Binary Phase Diagrams", Springer-Verlag, Berlin, FDR.

MORITA, Z. and TANAKA, T. (1983), *Trans. I.S.I.J.*, **23**, (10), 824-833.

MORITA, Z. and TANAKA, T. (1984), *Ibid.*, **24**, (3), 206-211.

PURDY, G. R. and KIRKALDY, J. S. (1971), *Metall. Trans.*, **2**, 371-378.

SCHURMANN, E., VON SCHWEINICHEN, J., VOLKER, R., and FISCHER, H.

(1987), *Giessereiforschung*, **39**, (3), 97-103 and 104-113.

SHARMA, R. and KIRKALDY, J. S. (1973), *Can. Met. Quart.*, **12**, 391-401.

STERENBOGEN, Yu. A. and PETROV., P. F. (1977), *Automat. Weld.*, **30**, 3–5.

STERENBOGEN, Yu. A., SHIRDENKO, N. I., and PETROV., P. F. (1976), *Ibid.*, **29**, 1–2.

STRANGWOOD, M. and BHADESHIA, H. K. D. H. (1987), "Welding Metallurgy of Structural Steels", *[Proc. Conf.]*, Ed., Jay Y. Koo, Met. Soc., Inc., Warrendale, PA 15086, 495-504.

SUGDEN, A. A. B. (1986), Dissertation submitted for Certificate of Postgraduate Study, University of Cambridge, U.K., Appendix I.

SWINDEN, D. J. and WOODHEAD, J. H. (1971), *J.I.S.I.*, **209**, (11), 883-899.

UHRENIUS, Bjørn (1978), "Hardenability Concepts with Applications to Steel", *[Proc. Conf]*, Eds., D. V. Doane and J. S. Kirkaldy, *Met. Soc. AIME*, AIMMPE, Warrendale, PA 15086, U.S.A., 28-81.

WAGNER, C. (1952), "Thermodynamics of Alloys", Addison-Wesley Publishing Co., London, U.K., 51-52.

WATANABE, Kazuo, (1975) *Tetsu-to Hagané*, **61**, 3069–3076.